AIAA JOURNAL
Vol. 46, No. 9, September 2008

Compressibility and Rarefaction Effects on Drag of a Spherical Particle

E. Loth*
University of Illinois at Urbana–Champaign, Champaign, Illinois 61801

DOI: 10.2514/1.28943

A review of compressibility and rarefaction effects on spherical particle drag was conducted based on existing experimental data, theoretical limits, and direct simulation Monte Carlo method results. The data indicated a nexus point with respect to effects of Mach number and Knudsen number. In particular, it was found that a single drag coefficient (of about 1.63) is obtained for all particle conditions when the particle Reynolds number is about 45, and is independent of compressibility or rarefaction effects. At lower Reynolds numbers, the drag is dominated by rarefaction, and at higher Reynolds numbers, it is dominated by compressibility. The nexus, therefore, allows construction of two separate models for these two regimes. The compression-dominated regime is obtained using a modification of the Clift–Gauvin model to specifically incorporate Mach number effects. The resulting model was based on a wide range of experimental data and showed superior prediction robustness compared with previous models. For the rarefaction-dominated regime, the present model was constructed to directly integrate the theoretical creeping flow limits, including the incompressible continuum flow limit (Stokes drag), the incompressible weak rarefaction limit (Basset–Knudsen correction), and the incompressible free-molecular flow limit (Epstein theory). Empirical correlations are used to extend this model to finite particle Reynolds numbers within the rarefaction-dominated regime.

I. Introduction

PARTICLE drag is related to the relative velocity of the particle. The particle velocity ($\mathbf{v}$) is defined as the translational velocity of the particle center of mass ($\mathbf{x}_p$). The gas velocity ($\mathbf{u}$) is the velocity far from the particle surface, which is uniform in the far field and which does not take into account the particle's presence. The relative velocity of the particles ($\mathbf{w}$) is then

$$\mathbf{w}(t) \equiv \mathbf{v}(t) - \mathbf{u}(t) \tag{1}$$

The quasi-steady drag force assumes steady flow, arises from pressure and viscous stresses applied to the particle surface, and resists the relative velocity $\mathbf{w}$. The dependence of drag on the magnitude of the relative velocity is primarily dictated by the particle Reynolds number (Re_p), defined as

$$Re_p = \frac{\rho_f |\mathbf{w}| d}{\mu_f} \tag{2}$$

In this expression, d is the particle diameter, ρ_f is the gas density, and μ_f is the gas viscosity. The particle Reynolds number is the nondimensional ratio of convective (fluid inertial) forces to viscous forces with respect to the fluid dynamics of the continuous phase in the vicinity of the particle.

When the particle Reynolds number is small ($Re_p \ll 1$), the viscous effects (as opposed to convective effects) dominate the fluid stress over the particle. This low Reynolds number condition is often called the "creeping flow" condition and leads to a fully attached laminar flow over the particle. Stokes [1] obtained the drag force in the limit of negligible convection terms and incompressible and continuum flow and showed that

$$\mathbf{F}_D = -3\pi d \mu_f \mathbf{w} \tag{3}$$

This is often referred to as the Stokes's drag regime owing to his derivation. This regime results in a linear dependence of drag on the relative velocity.

At high Reynolds numbers given by $2.0 \times 10^3 < Re_p < 3.0 \times 10^5$, a laminar boundary layer will form on the front of the particle ($\theta = 0$ deg) and will separate at $\theta \sim 80$ deg, producing a fully turbulent wake behind the particle. Because the pressure and shear stresses are proportional to the dynamic pressure, and the separation point is approximately constant, it can be expected that the resulting drag will be simply proportional to the dynamic pressure ($(1/2)\rho_f w^2$) and the particle frontal area ($\pi d^2/4$), and will be independent of viscosity changes. This leads to the well-known definition of the drag coefficient (C_D) written in terms of the total drag force as

$$\mathbf{F}_D \equiv -\frac{\pi}{8} d^2 \rho_f C_D w \mathbf{w} \tag{4}$$

Measurements have shown that C_D is approximately constant in this Re_p range (Fig. 1). This nearly constant value is called the "critical drag coefficient" ($C_{D,\text{crit}}$) with a value of about 0.4 to 0.45. This was recognized by Newton when he established the drag resistance for projectiles in 1710, and so that the associated Re_p range is often called the "Newton regime."

One may quantify the departure of the drag from the Stokes solution due to Reynolds number by normalizing the drag force by the creeping flow solution

$$f_{Re} \equiv \frac{F_D(Re_p)}{F_D(Re_p \to 0)} = \frac{C_{D,\text{Rep}}}{24/Re_p} \tag{5}$$

This ratio is called the "Stokes correction factor" and is equal to unity for $Re_p \ll 1$ and is proportional to Re_p for the Newton regime (approximately $3.0 \times 10^3 < Re_p < 2.0 \times 10^5$). At higher Reynolds numbers, the attached boundary layer becomes turbulent and causes the flow separation point to be shifted to a more aft position ($\theta \sim 120$ deg). Theses conditions are generally defined as having $Re_p > Re_{p,\text{crit}}$, where $Re_{p,\text{crit}}$ is termed the critical Reynolds number (approximately 3.0×10^5), which is generally defined when C_D drops below 0.3. Because particles are rarely at such high Re_p values, we will neglect the supercritical regime for our drag model. For intermediate particle Reynolds numbers (approximately $1.0 \times 10^{-1} < Re_p < 2.0 \times 10^3$), the flow behind the particle

Received 20 November 2006; revision received 6 March 2008; accepted for publication 23 March 2008.

*Professor, Aerospace Engineering, 306 Talbot Lab, 104 South Wright Street, Mail Code 236. Member AIAA.

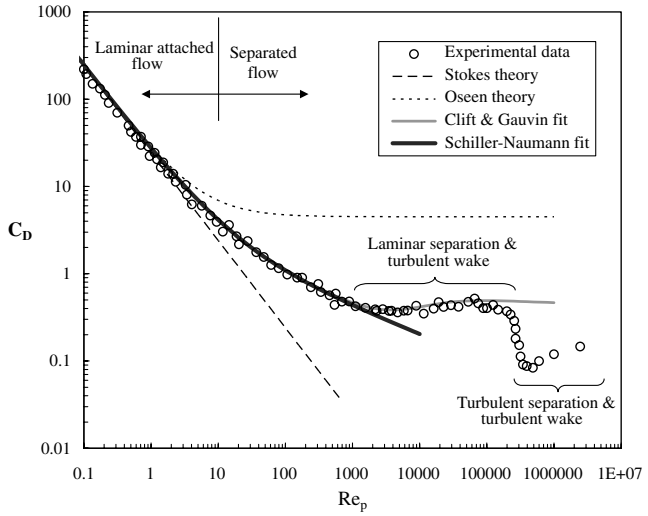

Fig. 1 Drag coefficient for a smooth solid sphere at various Reynolds numbers for incompressible flow conditions with experimental data reported in White [30].

transitions from an attached laminar wake, to a separated but still laminar wake, to an unsteady transitional wake (where the approach boundary layer is laminar).

Based on measurements of the drag coefficient for a wide range of Reynolds numbers as shown in Fig. 1, it can be seen that the flow transitions mentioned previously give rise to continuous but nonlinear variations. For the creeping flow regime, the drag coefficient based on the Stokes derivation is given as $C_D = 24/Re_p$, which is in good agreement with the experimental results for $Re_p \ll 1$ (e.g., less than 2% at an Re_p of 1.0×10^{-1}). Because there is no general analytical solution for intermediate Reynolds numbers, the intermediate conditions are generally prescribed by an empirical expression of the drag coefficient. There are a large number of curve fits, which have been proposed for the sphere correction data at higher Re_p values. For example, Clift et al. [2] gives a ten-part empirical curve set for sphere drag up to Re_p of 10^6, that is, the conditions include creeping flow and up to and past the drag crisis. A reasonable subcritical expression is given by Clift and Gauvin [3], which is accurate to within 6% of experiments (Fig. 1):

$$C_{D,\mathrm{Rep}} = \left[\frac{24}{Re_p}(1 + 0.15Re_p^{0.687})\right] + \frac{0.42}{1 + \frac{42{,}500}{Re_p^{1.16}}} \quad \text{for } Re_p < 2.0 \times 15^5 \tag{6}$$

The second term on the right-hand side (RHS) controls the transition to the critical drag coefficient set as 0.42. The first term on the RHS (in square brackets) is known as the Schiller–Naumann [4] drag expression and itself can be used for moderate Reynolds number as

$$f_{Re} = 1 + 0.15Re_p^{0.687} \quad \text{for } Re_p < 8.0 \times 10^2 \tag{7}$$

This "nonlinear drag" in the form of the Stokes correction is perhaps the most commonly used drag correction expression in multiphase flows because many particles are constrained to Re_p values in this range. Note that the drag given by Eqs. (6) and (7) represents the time-averaged component for $Re_p > 2.0 \times 10^2$ because some force unsteadiness results from the unsteady separated wake region.

II. Compressibility and Noncontinuum Parameters

To extend these results to include the effects of compressibility and rarefaction, the controlling nondimensional parameters should first be considered. The level of compressibility of the fluid can become important at high relative particle velocities compared with gas speed of sound (a_g). As such, the key parameter that describes compressibility is the Mach number, which is defined based on this ratio:

$$M_p \equiv \frac{w}{a_g} = \frac{w}{\sqrt{\gamma \mathcal{R}_g T_g}} \tag{8}$$

This assumes a thermally perfect gas with a fixed specific heat ratio (γ) and gas constant ($\mathcal{R}_g$). An incompressibility criterion can be written as

$$M_p \ll 1 \tag{9}$$

Compressibility will be significant when the relative Mach number is no longer small, for example, 0.4 or more. Such conditions are typically not expected based on terminal velocity. Instead, significant relative Mach numbers are generally due to particles interacting with high-speed flows. Examples include particles in a plasma spray or a rocket engine with a supersonic exit flow, particles ablating from a surface in a hypersonic boundary layer, and particles subjected to a shock wave. In these cases, the particle response time can lead to significant relative Mach numbers [5]. Thus, compressibility effects can be important to provide an understanding of the particle dynamics in such conditions.

To assess the validity of a continuum surrounding flow, the particle Knudsen number is defined as the ratio of mean free-path length of the surrounding molecules ($\mathcal{L}_{m-m}$) to the particle diameter. This can be written in terms of the particle Mach and Reynolds numbers for an ideal gas (Schaaf and Chambré [6]) as

$$Kn_p \equiv \frac{\mathcal{L}_{m-m}}{d} = \sqrt{\frac{\pi\gamma}{2}}\left(\frac{M_p}{Re_p}\right) \tag{10}$$

Small values of the Knudsen number ($<10^{-3}$) are consistent with a continuum approximation, whereby a very large number of molecular collisions occur at the particle surface, that is, the conventional no-slip boundary condition as assumed for the drag coefficients. The continuum criterion can be written as

$$Kn_p \ll 1 \tag{11}$$

Because gas viscosity and speed of sound typically have a modest variation with temperature, the continuum approximation is generally violated due to small particle size (e.g., diameters of 10 μ or less in atmospheric conditions) and/or low-density gases (e.g., near vacuum conditions or at very high altitudes).

When the constraint of Eq. (11) is violated so that Kn_p is no longer small, the flow around the particle can no longer be considered as a continuum. In this case, the molecules near the surface do not have a sufficiently high collision rate to ensure a mean velocity equal to that of the particle surface velocity, that is, the no-slip condition will not be realized. As a result, noncontinuum effects lead to a difference between the mean molecular velocity and the mean particle surface velocity, that is, a partial-slip condition. This phenomenon is referred to as "accommodation" and leads to the different regimes outlined in Table 1. For "slip" flow, the noncontinuum effect is weak and can be considered a small departure from the no-slip condition (allowing some theoretical analysis). Knudsen numbers much greater than unity are generally considered "free-molecular" flow conditions in which the molecules impact and reflect from the particle, but molecular–molecular interactions in the vicinity of the particle are negligible (theoretical analysis is again possible in this regime). The "transition" regime is in between these regimes and is the most complex to analyze.

Based on Eq. (10), one may generally consider the drag coefficient to be a function of two independent parameters (among M_p, Re_p, and Kn_p). At very high Reynolds numbers ($Re_p \gg 1$), the physics tends to be dominated by compressibility (M_p) because Kn_p will be generally small in these conditions. At very low Reynolds numbers, the physics will tend to be dominated by rarefaction (Kn_p) because M_p will be generally small in these conditions. These two regimes are illustrated in Fig. 2 (which was developed to summarize the predictions of present models) in terms of the drag coefficient for a sphere in thermal equilibrium, that is, $T_p = T_{g\infty}$. The trends (supported by experimental and numerical results) indicate a nexus

Table 1 Flow regimes based on Schaaf and Chambré (1961)

Knudsen range	Flow physics
$Kn_p \leq 0.01$	Continuum flow
$0.01 \leq Kn_p \leq 0.1$	Slip flow
$0.1 \leq Kn_p \leq 10$	Transition flow
$Kn_p \geq 10$	Free-molecular flow

of the compressibility and rarefaction effects at a single Reynolds number, that is

$$C_D \approx 1.63 \quad \text{at} \quad Re_p = 45 \quad \text{for all } M_p \quad \text{and} \quad Kn_p \tag{12}$$

The independence of compression or rarefaction at this condition (for thermal equilibrium) was qualitatively noted by Zarin [7]. This condition corresponds to a particle with a steady separated wake in the incompressible continuum limit. Unfortunately, the corresponding flow is not analytically tractable. As such, it is not clear whether the lack of influence for Mach number and Knudsen number is caused by 1) a limit in which Re_p is too small to have significant compressibility effects but Re_p is too large to have significant rarefaction effects, or 2) a limit in which the compressibility effects and rarefaction effects are effectively counteractive. The former would suggest that viscous effects are much stronger than either compressibility effects or rarefaction effects at this condition. Qualitatively, this may be a reasonable assumption because shock waves do not form as strong discontinuities at such Reynolds numbers. However, it is expected that the latter cause is the reason because the flow field around a particle at Re_p of 45 can be expected to be markedly different in free-molecular flow as compared with continuum conditions. More research is needed to examine the detailed flow physics around a particle at this condition to properly address, if and why the rarefaction and compressibility effects counteract.

In either case, the appearance of the nexus condition can be exploited to provide a robust prediction of the drag by considering separate models for $Re_p < 45$ (where rarefaction effects are know to dominate because typical M_p values are small) and for $Re_p > 45$ (where compressibility effects are known to dominate because typical Kn_p values are small). Thus, the Fig. 2 predictions of C_D in the rarefaction-dominated regime will be developed separately from those in the compression-dominated regime. In the following, the compression-dominated regime is first considered, followed by the rarefaction-dominated regime for which temperature differences can be important. Finally, the thermophoretic force associated with temperature gradients (which can be significant in the rarefaction-dominated regime) is considered.

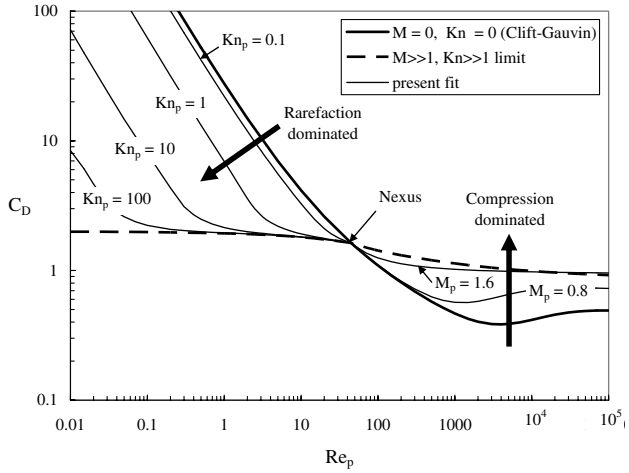

Fig. 2 Rarefaction and compression effects on drag of a spherical particle with $T_p = T_{g\infty}$ in which present fit corresponds to Eqs. (14–16) for $Re_p > 45$ and Eqs. (22–27) for $Re_p < 45$.

III. Compression-Dominated Regime

Various compressible flow features will determine the flowfield over a sphere, depending on the Mach number (Fig. 3). The compression-dominated regime generally yields increased drag as the Mach number increases (recall Fig. 2). The change in the drag coefficient due to compressibility can be expressed in terms of a drag ratio defined as

$$C_M \equiv \frac{C_{D,\text{crit}}}{C_{D,\text{crit},M=0}} \tag{13}$$

As with the drag ratio for shape effects, the baseline (incompressible) critical drag coefficient is taken as 0.42.

The increase in drag is initially due to the influence of compressibility on boundary layer separation for $M_p > 0.2$ (Schlichting [8]), but this effect is generally mild. At higher Mach numbers, the maximum flow velocity around the sphere (at $\theta = 90$ deg according to potential flow theory) will eventually reach a sonic speed. The freestream Mach number associated with this condition is defined as the critical Mach number (M_{crit}), approximately 0.6 for a sphere (Hoerner [9]). Beyond this speed, gas dynamic waves appear. For example, flow at a subsonic but supercritical Mach number is shown in Fig. 3a, where one can see weak expansion waves as the flow becomes locally supersonic, followed by a lamda-shock pattern at the top of the sphere. This boundary layer shock interaction promotes earlier flow separation than that seen for the incompressible condition. As a result, the drag significantly increases for $M_p > M_{\text{crit}}$ (Fig. 4).

As the Mach number becomes supersonic, a bow shock forms in front of the sphere (Fig. 3b) but the point of flow separation moves further back because there is no longer a lamda shock present. The corresponding drag initially increases until it is maximized at about M_p of 1.5 (Fig. 4). At higher Mach numbers, the flow retains a bow shock but the stand-off distance is reduced, and boundary layer separation is further delayed due to supersonic expansion over the rear portion (Fig. 3c). As a result, the drag ratio is somewhat reduced and eventually approaches a constant at hypersonic Mach numbers $C_{M\to\infty} \approx 2$ (Fig. 4). Because the rear flow separation is primarily dictated by the gas dynamics, the flow and the drag coefficient are not sensitive to Re_p for $M_p > 1.5$, that is, there is no "drag crisis" when the boundary transitions from laminar to turbulent conditions. As a result, Crowe [10] termed the supersonic C_D as the "inviscid drag coefficient" because boundary layer properties have little influence. There is no theoretical correction for Mach number effects at these conditions, and so the drag ratio must be described empirically. Herein, the drag ratio is modeled based on the available experimental data of Fig. 4 as a two-part expression:

$$C_M = \tfrac{5}{3} + \tfrac{2}{3}\tanh[3\,\ell_n(M_p + 0.1)] \quad \text{for } M_p \leq 1.45 \tag{14a}$$

$$C_M = 2.044 + 0.2\exp\{-1.8[\ell_n(M_p/1.5)]^2\} \quad \text{for } M_p \geq 1.45 \tag{14b}$$

This is similar to the fit given by Crowe et al. [11] and yields the same trends, that is, Mach number effects are generally weak below the critical Mach number ($M_p < 0.6$), whereas a nearly constant drag coefficient is found in the hypersonic regime ($M_p > 5$).

To represent the influence of Mach number between the nexus point (at which the effect is negligible) and the high Re_p regime [where the effect is given by Eq. (14)], it is convenient to employ a modified Clift–Gauvin drag expression in the following form:

$$C_D = \frac{24}{Re_p}\left[1 + 0.15Re_p^{0.687}\right]H_M + \frac{0.42C_M}{1 + \frac{42{,}500G_M}{Re_p^{1.16}}} \quad \text{for } Re_p > 45 \tag{15}$$

This expression involves the critical drag coefficient ratio defined in Eq. (13) so that it recovers the trends of Fig. 4 at high Reynolds numbers. To incorporate the reduction of compressibility effect as the Reynolds number is reduced, Eq. (15) introduces two empirical

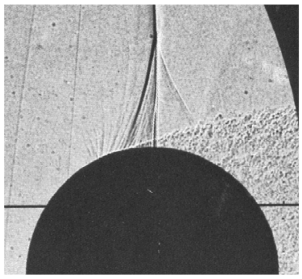

a)

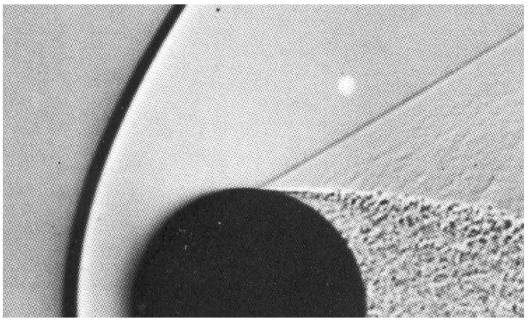

b)

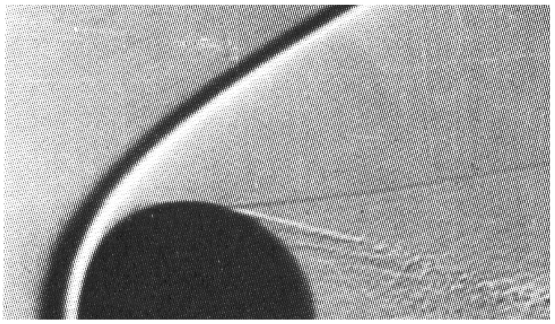

c)

Fig. 3 Shadowgraphs of spheres from Van Dyke [31] with very high particle Reynolds numbers (approximately 9.0×10^5) at a) $M_p = 0.86$, b) $M_p = 1.53$, and c) $M_p = 3$. (Figure included with permission of Parabolic Press.)

functions of the particle Mach number given by

$$G_M = 1 - 1.525M_p^4 \quad \text{for } M_p < 0.89 \tag{16a}$$

$$G_M = 0.0002 + 0.0008\tanh[12.77(M_p - 2.02)] \quad \text{for } M_p > 0.89 \tag{16b}$$

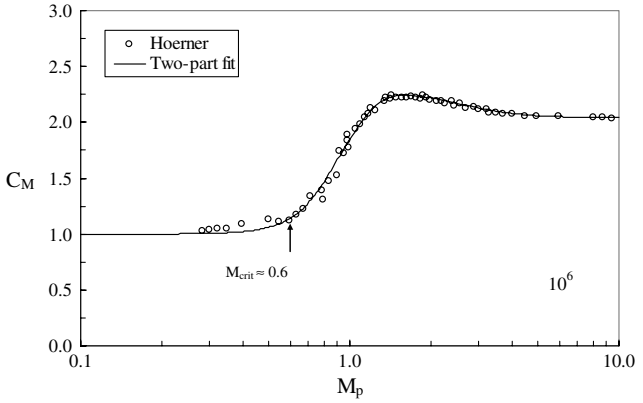

Fig. 4 Mach-based drag ratio at $Re_p > 1.0 \times 10^4$ based on data of Hoerner [9] and Eq. (14).

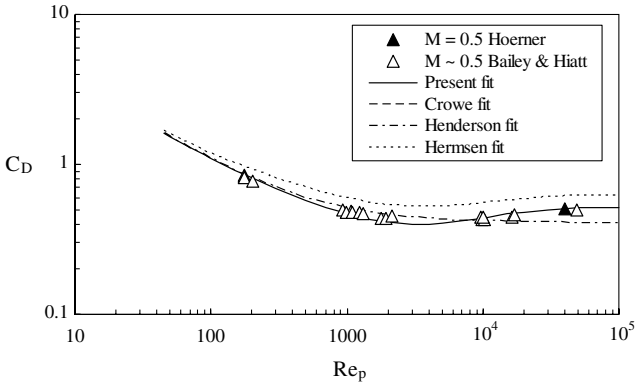

Fig. 5 Prediction of the drag curve at $M_p \sim 0.5$ for various models in which present fit corresponds to Eqs. (14–16).

$$H_M = 1 - \frac{0.258C_M}{1 + 514G_M} \tag{16c}$$

The form of H_M is constructed to ensure that the nexus of Eq. (12) is satisfied, while G_M is constructed to ensure that the resulting form recovers the incompressible Clift–Gauvin limit as M_p approaches zero. As shown in Fig. 5, this model is more accurate than previous models in terms of predictive performance for a range of Reynolds numbers, M_p, while the robustness in terms of Mach number is demonstrated in Fig. 6.

IV. Rarefaction-Dominated Regime

The effect of rarefaction becomes important for finite Knudson numbers and low Reynolds numbers as discussed in the preceding section. When the flow is in continuum (Eq. (11) satisfied), the drag force for a spherical particle given by the Schiller–Naumann expression of Eq. (7) is reasonable (for $Re_p < 45$). For finite Knudsen numbers but small Reynolds numbers, a Stokes correction can be defined as

$$f_{Kn} \equiv \frac{F_D(Kn_p, Re_p \ll 1)}{3\pi\mu_f d} \tag{17}$$

This expression is often referred to as the Cunningham correction factor and depends on the surface properties. For a smooth particle, the angles of incidence and reflection at the molecular length scales will be equal (specular reflection), and the tangential momentum will be conserved. For a rough particle, the normal velocity component is assumed zero, whereas the molecular reflection will be random (diffuse reflection), and some portion of the tangential momentum will be lost. For small but finite Knudsen numbers, the boundary condition for the tangential surface velocity (u_θ) was expressed by Talbot et al. [12] in terms of the velocity gradients, the surface temperature gradient, and a tangential momentum coefficient (c_θ), which, in turn, is defined in terms of the accommodation coefficient (c_{accom}):

$$u_\theta \approx c_\theta \mathcal{L}_{m-m}\left[\frac{1}{r}\frac{\partial u_r}{\partial \theta} - r\frac{\partial}{\partial r}\left(\frac{u_\theta}{r}\right)\right]_{r=r_p} + c_\theta\left(\frac{\nu_g}{\mathcal{R}_g T_g}\right)\left(\frac{\partial T_g}{\partial \theta}\right)_{r=r_p} \tag{18a}$$

$$c_\theta \equiv (2 - c_{\text{accom}})/c_{\text{accom}} \tag{18b}$$

The accommodation coefficient, c_{accom}, is the fraction of molecules that undergo diffuse reflection upon impacting the particle, whereas the remaining fraction undergoes specular reflection. As such, $c_{\text{accom}} \leq 1$, and a typical value is about 0.9 on most surfaces. This corresponds to $c_\theta \approx 1.22$, though this coefficient can range from 1.0 to 1.5. For the RHS of Eq. (18a), Talbot et al. [12] also pointed out that the c_θ value used for the velocity term may be different from that

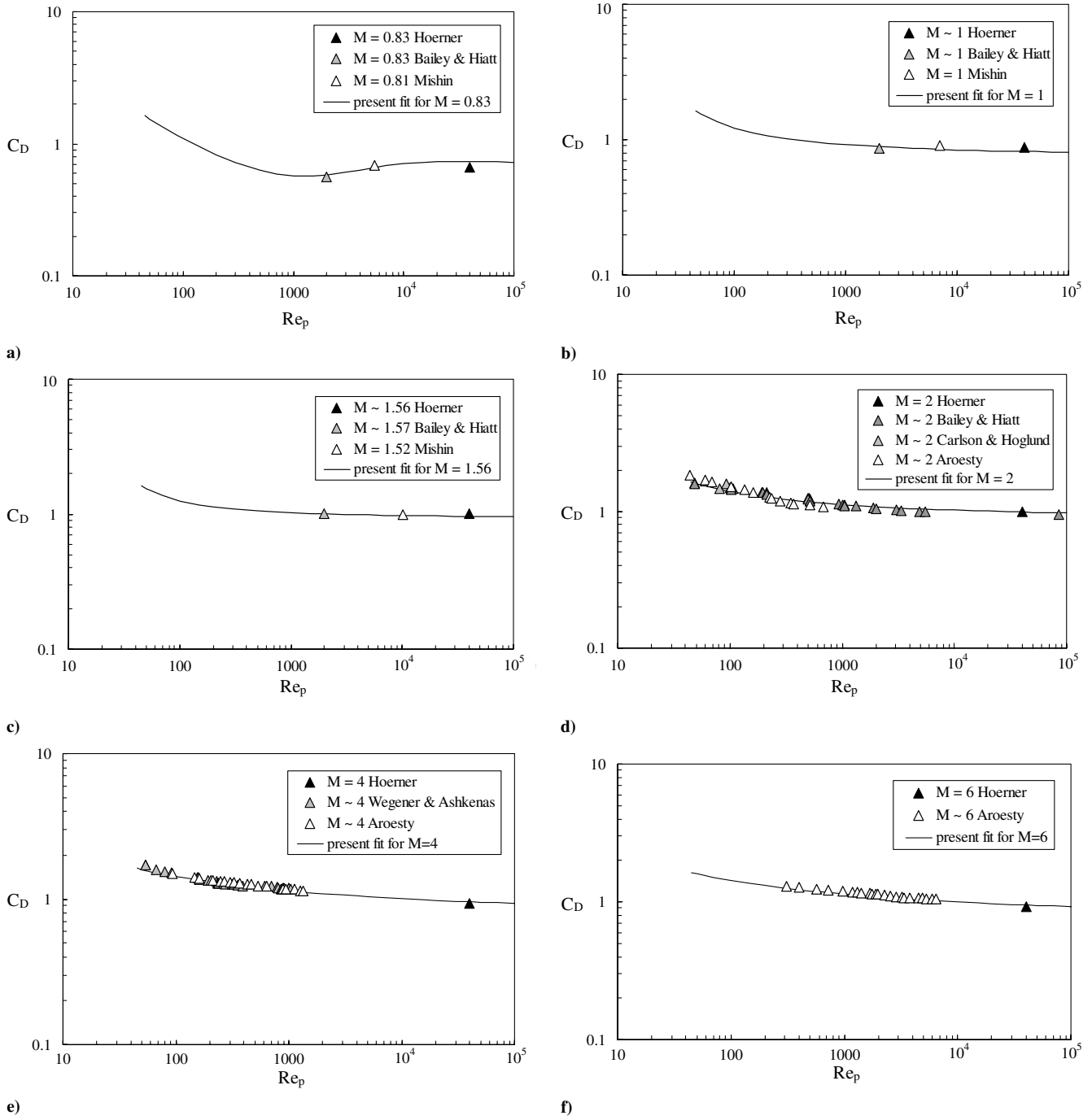

Fig. 6 Drag coefficient as a function of Reynolds number for various Mach numbers based on data of Wegener and Ashkenas [32], Aroesty [24], Carlson and Hoglund [21], Hoerner [9], Bailey and Hiatt [25], and Mishin [33]: a) $M_p \sim 0.8$, b) $M_p \sim 1$, c) $M_p \sim 1.5$, d) $M_p \sim 2$, e) $M_p \sim 4$, and f) $M_p \sim 6$ [present fit corresponds to Eqs. (14–16)].

used for temperature term. However, the difference is typically quite small, approximately 3%, and so that a single value of c_θ, as used herein, is generally reasonable.

Assuming weak temperature gradients so that the second term of Eq. (18a) can be neglected, Basset [13] theoretically obtained the Knudsen correction factor for slip flow

$$f_{Kn} = 1 - 2c_\theta Kn_p + O\left(Kn_p^2\right) \quad \text{for } Kn_p \ll 1 \tag{19}$$

In the other limit of free-molecular flow ($Kn_p \gg 1$), Epstein [14] obtained a theoretical result by assuming that the velocity distribution of the molecules striking the sphere is based on a Maxwell distribution (and unaffected by the presence of the sphere), yielding

$$f_{Kn} \to \frac{8 + 2\pi/(c_\theta + 1)}{36 Kn_p} \quad \text{for } Kn_p \gg 1 \tag{20}$$

Combining this correction factor (which is inversely proportional to Kn_p) with its definition [Eq. (17)] and Eq. (10) indicates that the drag force is independent of viscosity in the free-molecular flow limit. This is because the molecular velocity distribution is no longer Maxwellian because binary collisions are no longer the dominant process for exchange of energy between the gas molecules. Note that some references (e.g., Clift et al. [2]) give a result which has a factor of 2 error in this and some of the subsequent equations, presumably due to conflicting definitions of Knudsen number (herein, it is based on particle diameter, though early studies based it in on particle radius).

To bridge the gap from very low to very high Knudsen numbers, Phillips [15] proposed an approximate theoretical solution, which assumed low Re_p and M_p but allowed for intermediate Knudsen number values

$$f_{Kn} = \frac{15c_\theta - 6c_\theta^2 Kn_p + (16 + 16c_\theta + 4\pi)\left(c_\theta^2 + 2\right)Kn_p^2}{15c_\theta + 24c_\theta^2 Kn_p + 36c_\theta\left(c_\theta^2 + 1\right)Kn_p^2 + 72\left(c_\theta^2 + 2\right)(c_\theta + 1)Kn_p^3} \tag{21}$$

Because particle accommodation coefficients are not generally known to high accuracy, general empirical representations have been put forth. A reasonably accurate expression is that discussed by Clift et al. [2], which is consistent with $c_\theta \approx 1.22$:

$$f_{Kn} = \frac{1}{1 + Kn_p[2.514 + 0.8\exp(-0.55/Kn_p)]} \tag{22}$$

In the limit of particle Reynolds and Mach numbers much less than unity, both the theoretical and empirical expressions [Eqs. (21) and (22)] show that the slip effect results in decreasing equivalent drag as the Knudsen number increases. As shown in Fig. 7, both expressions also compare favorably with the experimental data of Millikan [16,17]. Also shown in this figure is the direct simulation Monte Carlo (DSMC) data of Benson et al. [18], which follows the trends as well. To account for finite Reynolds numbers, the Knudsen number effect described here can be extended by including a Schiller–Naumann correction as

$$C_{D,Kn,Re_p} = C_{D,\mathrm{Rep}} f_{Kn} = \frac{24}{Re_p}\left(1 + 0.15Re_p^{0.687}\right)f_{Kn} \tag{23}$$

This expression, which will be shown to be quite robust, can use either a theoretical or an empirical Knudsen correction [e.g., Eq. (21) or Eq. (22)], but assumes the particle Mach number is small. Note that use of the drag coefficient form, instead of the drag correction form, is more appropriate in free-molecular flow for which the drag is no longer proportional to viscosity.

As the particle Mach number becomes significant, for example, of order unity or more, a free-molecular creeping flow limit can be obtained in terms of the molecular speed ratio

$$s \equiv M_p\sqrt{\gamma/2} \tag{24}$$

Assuming equal tangential and normal accommodation coefficients, Stadler and Zurick [19] and Schaaf and Chambré [6] derived the inviscid free-molecular compressibility limit for $s > 1$ (approximate supersonic flow) as

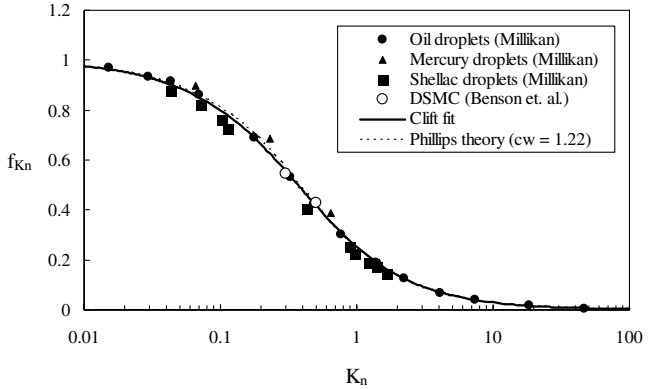

Fig. 7 Knudsen number effects on the Stokesian drag correction for $Re_p \ll 1$ and $M_p \ll 1$ with predictions of Phillips [15] [Eq. (21)] and Clift et al [2] [Eq. (22)].

$$C_{D,\mathrm{fm}} = \frac{(1 + 2s^2)\exp(-s^2)}{s^3\sqrt{\pi}} + \frac{(4s^4 + 4s^2 - 1)\mathrm{erf}(s)}{2s^4} + \frac{2}{3s}\sqrt{\pi\frac{T_p}{T_\infty}} \tag{25a}$$

The first two terms refer to the diffuse reflection, whereas the third term refers to specular reflection, which includes the effect of the particle temperature ratio. This ratio is based on T_∞, which is the far-field gas temperature as seen by the particle, that is, the "uncoupled" gas temperature hypothetically extrapolated to the particle centroid ($T_{f@p}$). This is normally equal to the particle temperature for thermal equilibrium conditions, but T_p may be different than the ambient temperature if the particle is undergoing rapid heating or cooling (e.g., due to injection conditions, shock passage, etc.). Hersch et al. [20] noted that the form of Eq. (25a) is equal to the Epstein [14] model if one assumes that the thermal accommodation coefficient is equal to the momentum accommodation coefficient. The free-molecular drag coefficient for equilibrium particle temperature is defined as

$$C'_{D,\mathrm{fm}} = C_{D,\mathrm{fm},T_p=T_\infty} = \frac{(1 + 2s^2)\exp(-s^2)}{s^3\sqrt{\pi}} + \frac{(4s^4 + 4s^2 - 1)\mathrm{erf}(s)}{2s^4} \tag{25b}$$

In the limit of very high speed ratios, this gives $C'_{D,s\gg1} = 2$, which is often taken as the lower limit for low Reynolds number drag.

The free-molecular limit can be empirically corrected for finite Reynolds numbers by ensuring that the nexus given by Eq. (12) is satisfied (regardless of particle temperature) with

$$C_{D,\mathrm{fm},Re} = \frac{C_{D,\mathrm{fm}}}{1 + \left(\frac{C'_{D,\mathrm{fm}}}{1.63} - 1\right)\sqrt{\frac{Re_p}{45}}} \tag{26}$$

In this case, the limit of very high speed ratios and equilibrium particle temperature but finite Reynolds numbers becomes

$$C'_{D,s\gg1,Re} = (0.5 + 0.0169\sqrt{Re_p})^{-1}$$

which is often taken as the lower limit for low Reynolds number drag. This limit and the creeping free-molecular limits of Eq. (25b) are shown in Fig. 8, where it can be seen that there is a substantial difference between the free-molecular values and the continuum Clift–Gauvin drag coefficient, especially at small particle Reynolds numbers.

Whereas the free-molecular compressibility limit is appropriate for $s \geq 1$ (including hypersonic conditions), it becomes undefined (infinite) for the zero Mach number limit. To additionally blend the finite Mach number limit with the zero Mach number limit, the following empirical combination is proposed for the overall drag coefficient:

$$C_D = \frac{C_{D,Kn,Re}}{1 + M_p^4} + \frac{M_p^4 C_{D,\mathrm{fm},Re}}{1 + M_p^4} \quad \text{for } Re_p \leq 45 \tag{27}$$

This expression represents the overall fit to the rarefaction regime and simultaneously allows for Reynolds, Mach, Knudsen, and temperature ratio effects for the rarefaction-dominated regime. For the low Mach number conditions of Fig. 7, this model reverts identically to the f_{kn} expression of Eq. (22), which reverts to the correct theoretical limits of Eqs. (19) and (20). For the finite Mach number conditions, this model also correctly asymptotes to the free-molecular limit (shown by the dashed lines in Fig. 8), including the limit of $s \gg 1$, where $C_D \to 2$. This model also properly represents Reynolds number effects as shown by comparison with experimental and DSMC data in Fig. 8. Because of these attributes, the present model consistently outperforms those of Carlson and Hoglund [21], Crowe [10], Henderson [22], and Hermsen [23] in the rarefaction-dominated regime, for example, as shown in Fig. 9.

Temperature ratio effects are also included in the present model via the specular term of Eq. (25). As shown in Fig. 10a, this leads to

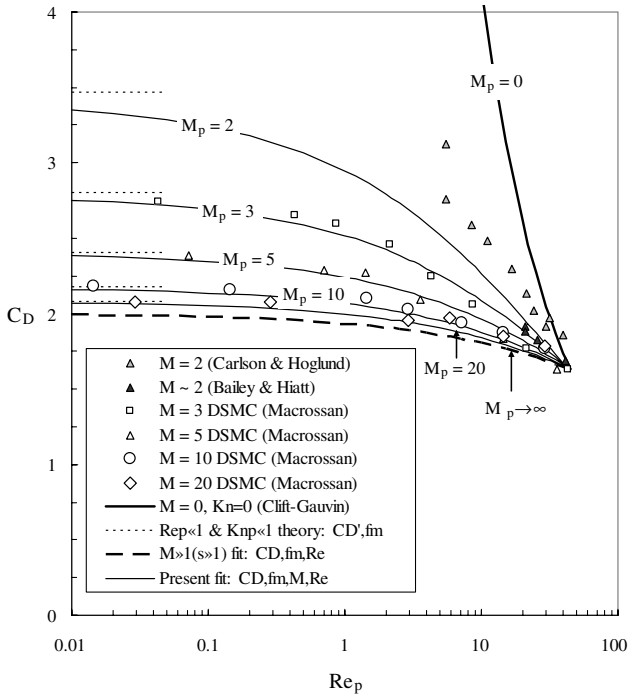

Fig. 8 Compression effects for rarefaction regime ($Re_p < 45$), based on data of Carlson and Hoglund [21], Bailey and Hiatt [25], and Macrossan [34], where $M = 0$ and $Kn = 0$ is based on Eq. (6), free-molecular theory is given by Eq. (25), $M \gg 1$ and $Kn \gg 1$ is based on lower limit of Eq. (26), where $C_{D,\mathrm{fm}}$, is based on Eq. (25), $C_{D\mathrm{frm,Re}}$ is based on Eq. (26), and present fit is based on Eqs. (22–27).

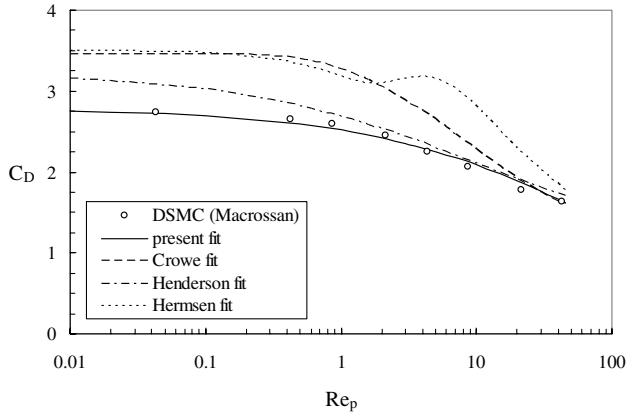

Fig. 9 Drag coefficient in the rarefaction-dominated regime at $M_p = 2.95$, where present fit is based on Eqs. (22–27).

increases in drag as the particle temperature increases due to an additional viscous contribution. The effect is highest at the creeping compressible flow limit [where the model reverts to Eq. (25)] and reduces as the Re_p increases. For all these conditions, the present drag model gives the best prediction of the temperature influence, and a typical comparison with previous models is shown in Fig. 10b. Beyond the nexus point (in the compression-dominated region), little data is available to support whether the temperature increases or decreases the drag, but, in general, the effect of T_p/T_∞ is small (Aerosty [24]; Bailey and Hiatt [25]).

V. Thermophoretic Forces

The thermophoretic effect is caused by temperature gradients in the continuous fluid surrounding the particle. It arises due to the gradient of the kinetic energy of the surrounding molecules and can be significant (compared with drag) for noncontinuum conditions, for example, in small particles in gasses. In particular, the "hot side"

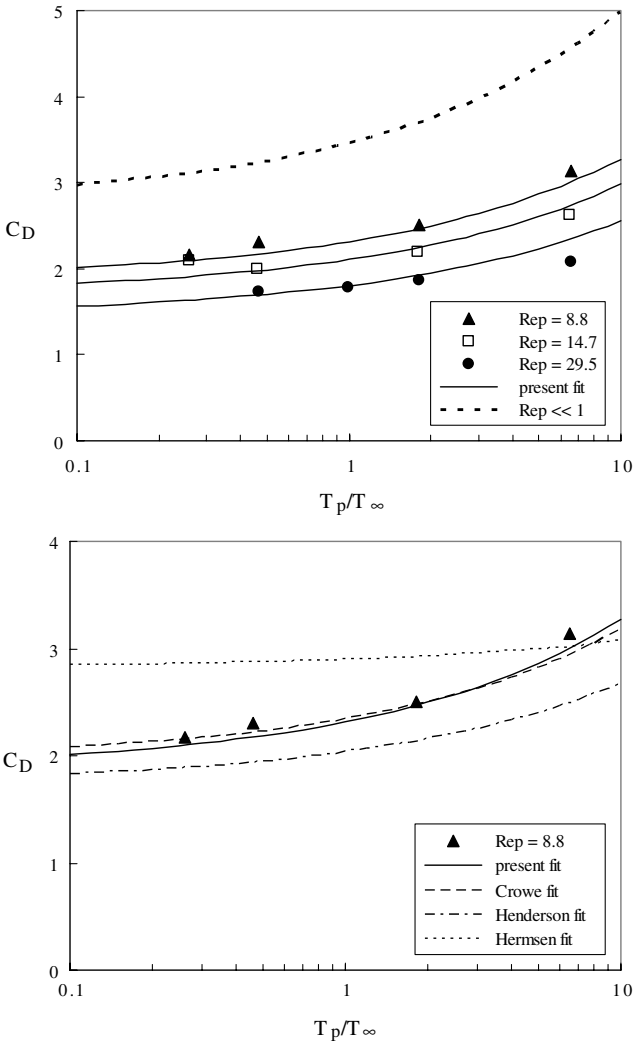

Fig. 10 Influence of particle temperature ratio at $M_p = 2$ based on data of Bailey and Hiatt [25] a) for various particle Reynolds numbers, and b) predicted by various models [present fit is based on Eqs. (22–27)].

of a particle experiences collisions from molecules with higher velocities as compared with that of the cool side according to kinetic gas theory (Fig. 11). The net result yields a force in the direction opposite to the temperature gradient. Thermophoresis can be used to drive particles away from a hot wall or toward a cold wall; the sooting of kerosene lamps is an example of the latter. The fabrication of microprocessors depends on thermophoresis because the repulsion and or deposition of impurities on the wafer is controlled during elevated temperature conditions. In addition, this phenomenon is used in thermal precipitators to filter submicron-sized particles from gas flows. Thermophoretic forces can also play an important role in plasma flows, combustors, and heat exchangers.

The thermophoretic force is generally written as a function of the particle Knudsen number (Kn_p) as defined in Eq. (10). As with drag in rarefied flows, thermophoresis has three primary regimes: near continuum ($Kn_p \ll 1$), transition ($Kn_p \sim 1$), and free molecular ($Kn_p \gg 1$). Similarly, there are theoretical approaches for the extreme cases, whereas the transition regime is generally modeled with empirical relations based on experiments and resolved simulations. A second influential parameter is the ratio of the gas-to-particle thermal conductivities:

$$\mathcal{K}^* \equiv \frac{\mathcal{K}_g}{\mathcal{K}_p} = \frac{15\mu_g \mathcal{R}_g}{4\mathcal{K}_p} \tag{28}$$

If the particle thermal conductivity is small compared with the gas ($\mathcal{K}^* \gg 1$), then it will have an interior temperature gradient that

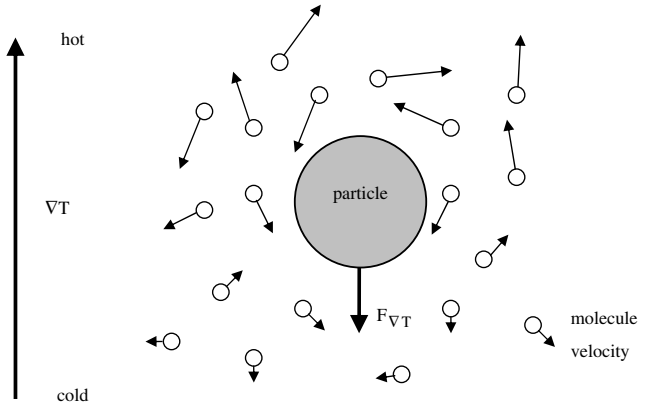

Fig. 11 A particle surrounded by a gas with a temperature gradient creates a thermophoretic force on the particle.

approaches that of the surrounding flow for near-continuum conditions. However, most gas/particle combinations are best described by $\mathcal{K}^* \ll 1$ for which the particle's internal temperature field is more uniform, resulting in increased temperature differences between the particle and the gas at the interface. Various models for the force are considered next for steady-state conditions.

For the near-continuum regime, one of the earliest approaches for the thermophoretic force was presented by Epstein [14]. However, the first analysis to formally allow for small $\mathcal{K}^*$ conditions was completed by Brock [26] using the surface boundary condition with tangential accommodation [Eq. (18)]. Brock assumed a uniform temperature gradient in the far field and imposed a heat flux boundary condition on the sphere surface based on the ratio of the thermal conductivity of the gas to that of the particle, expressed as

$$\mathcal{K}^* \equiv \frac{\mathcal{K}_g}{\mathcal{K}_p} = \frac{15\mu_g \mathcal{R}_g}{4\mathcal{K}_p} \tag{29}$$

The gas and the particle temperature fields were assumed to satisfy Laplace's equation with a temperature-jump boundary condition at $r = r_p$ given by

$$T_g = T_p + c_T \mathcal{L}_{m-m}(\partial T_g/\partial r)$$

where c_T is a temperature accommodation coefficient, approximately 2.18 (Loyalka [27]). Using the Stokes stream function, the Brock's force due to thermophoresis is

$$F_{\nabla T, Kn_p \ll 1} = -\frac{6\pi\mu_g \nu_g d(\frac{2-c_\theta}{c_\theta})(\mathcal{K}^* + 2Kn_p c_T)}{[1 + 6Kn_p(\frac{2-c_\theta}{c_\theta})](1 + 2\mathcal{K}^* + 4Kn_p c_T)} \left(\frac{\nabla T_g}{T_g}\right)_{@p} \tag{30}$$

The negative sign indicates a force opposing the unhindered gas temperature gradient, that is, the gradient which would exist in the absence of the particle. Talbot et al. [12] noted that this theory is reasonable for near continuum ($Kn_p \ll 1$), at which point it yields a force that is approximately linearly proportional to Kn_p (as noted by the previous expression). As such, thermophoresis becomes more important as particles become smaller (approximately 10 μor less) or the gas pressure decreases.

The large Knudsen number ($\mathcal{L}_{m-m} \gg d$) limit can be obtained assuming no collisions between molecules, as was employed for free-molecular drag theory mentioned previously. The result by Waldmann [28] for monatomic gases is

$$F_{\nabla T, Kn_p \gg 1} = -\frac{\pi}{2}\mu_g \nu_g \frac{d}{Kn_p}\left(\frac{\nabla T_g}{T_g}\right)_{@p} \tag{31}$$

It turns out that Brock's theory [Eq. (30)] approaches the free-molecular limit [Eq. (31)] in the limit of $Kn_p \gg 1$ but, unfortunately, is not accurate for intermediate Kn_p conditions, as will be discussed next. However, this indicates that the intermediate regime may (and indeed does) have a similar linear dependence on the gas viscosity,

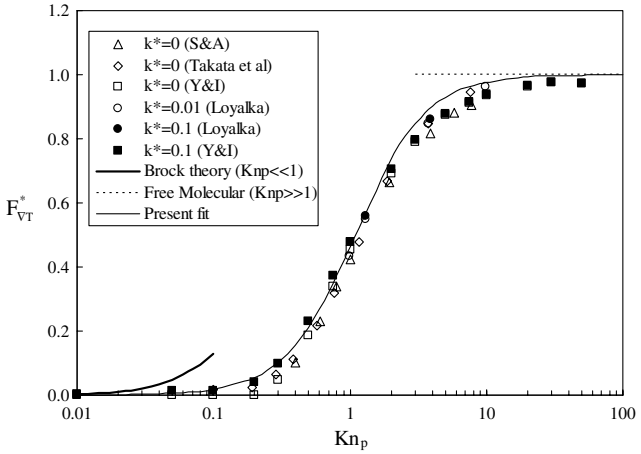

Fig. 12 Thermophoretic force as a function of particle Knudsen number for various predictions and for resolved-surface simulations of Sone and Aoki [35], Yamamato and Ishihara [36], Loyalka [27], and Takata et al. [37]. Data are grouped as $\mathcal{K}^* \leq 0.01$ (open symbols) or as $\mathcal{K}^* \geq 0.1$ (filled symbols) and Brock theory given by Eq. (30), free-molecular limit is given by Eq. (31), and present fit is based on Eqs. (31–33).

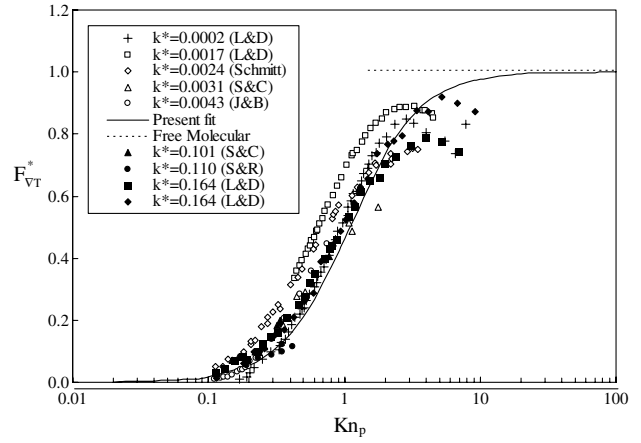

Fig. 13 Comparison of nondimensional thermophoretic force predictions with experimental data (Saxton and Ranz [38], Schmitt [39], Schadt and Cadle [40], Jacobson and Brock [41], and Li and Davis [42], with data grouped as in Fig. 12, and present fit is based on Eqs. (31–33).

particle diameter, and gas thermal gradient so that it is appropriate to consider a normalized thermophoretic force based on the free-molecular limit, which itself should only be a function of Kn_p and $\mathcal{K}^*$:

$$F^*_{\nabla T} \equiv \frac{F_{\nabla T}}{F_{\nabla T, Kn_p \gg 1}} \tag{32}$$

To observe the detailed dependence on Kn_p for the intermediate regime, one may consider data from resolved-surface simulations based on the Boltzmann–Krook–Welander (BKW) and Bhatnagar–Gross–Krook (BGK) models of the Boltzmann equation. Data from such simulations are shown in Fig. 12 for the nondimensionalized force. The results indicate that the force is a strong function of the Knudsen number but only a weak function of the conductivity ratio. Generally, the Brock theory is appropriate for $Kn_p < 0.01$, whereas the free-molecular theory is appropriate for $Kn_p > 20$.

As discussed by Zheng [29], there have been several models of various levels of complexity, which have proposed to describe the intermediate Kn_p functional dependence in terms of $\mathcal{K}^*$, c_θ, and/or c_T. However, a simple model which neglects the secondary parameters and gives reasonable agreement with the resolved-surface simulations is given by

$$F^*_{\nabla T} \equiv \frac{Kn_p^{1.7}}{1.15 + Kn_p^{1.7}} \quad \text{for } Kn_p > 0.01 \tag{33}$$

In Fig. 13, this model is compared with experimental data in various gasses (air, argon and helium) with conductivity ratios ($\mathcal{K}^* \sim 0.1$) and low conductivity ratios ($\mathcal{K}^* \ll 1$). Though there is considerable spread in the data and perhaps some evidence of a $\mathcal{K}^*$ dependence, the simple empirical fit yields good agreement for Kn_p greater than 0.01 for all the conductivity ratios studied. In contrast, the Brock theory tends to overestimate the force for Kn_p greater than 0.01 (by about four fold), and, unfortunately, there is little experimental data at lower Kn_p values, where it is expected that the $\mathcal{K}^*$ dependence will be more significant. However, the force is generally negligible in this regime, and so this issue may not be of substantial practical importance.

VI. Conclusions

A new model of the drag of spherical particles subjected effects of compressibility and rarefaction was developed. It is based on the observation of a nexus point at a particle Reynolds number of 45, where the drag coefficient is approximately 1.63, independent of Mach and Knudsen numbers for particles in thermal equilibrium with the surrounding gas. This yields a model defined by two regimes: compression dominated for $Re_p > 45$ with Eqs. (14–16) and rarefaction dominated for $Re_p < 45$ with Eqs. (22–27).

For the compression-dominated regime, the experimental data and the empirical correlation indicate that Mach number effects are generally weak below the critical Mach number ($M_p < 0.6$), whereas a nearly constant drag coefficient is found in the hypersonic regime ($M_p > 5$). For the rarefaction-dominated regime, the present model directly incorporates all the relevant theoretical limits in the rarefaction-dominated regime (an attribute not found in most previous models). It also correlates well with experimental data and DSMC for finite particle Reynolds numbers, with improved predictive performance in terms of accuracy and robustness compared with previous models. However, the models do not incorporate effects of unsteadiness or nonsphericity. Further research is needed to understand whether the nexus conditions corresponds to 1) a limit at which Re_p is too small to have significant compressibility effects, whereas Re_p is too large to have significant rarefaction effects, or 2) a limit at which the compressibility effects and rarefaction effects are effectively counteractive.

A related investigation into the thermophoretic force noted that the effects of temperature gradient for incompressible noncontinuum conditions were not substantially sensitive to gas-to-particle conductivity ratios and particle surface accommodation coefficients. Based on this, a model for the thermophoretic force was developed for a wide variety of Knudsen numbers as given by Eqs. (31–33). This model agrees well with resolved-surface simulations and experimental data while tending to the correct theoretical limits, but does not account for heat or mass transfer effects.

Acknowledgments

The author would like to thank Patrick Woo for creating the figures as well as assisting in the data collection and analysis. The comments and suggestions by the reviewers were also appreciated.

References

[1] Stokes, G. G., "On the Effect of the Internal Friction of Fluids on the Motion Of Pendulums," *Transactions of the Cambridge Philosophical Society (Mathematical and Physical Sciences)*, Vol. 9, Pt. 2, 1851, pp. 8–106.

[2] Clift, R., Grace, J. R., and Weber, M. E., *Bubbles, Drops and Particles*, Academic Press, New York, 1978.

[3] Clift, R., and Gauvin, W. H., *Proceedings of CHEMECA '70*, Vol. 1, Butterworth, Melbourne, 1970, pp. 14–28.

[4] Schiller, L., and Naumann, A. Z., "Über die Grundlegenden Berechungen bei der Schwerkraftaufbereitung," *Zeitschrift des Vereines Deutscher Ingenieure*, Vol. 77, No. 12, 1933, pp. 318–320.

[5] Sivier, S. A., Loth, E., Baum, J. D., and Lohner, R., "Unstructured Adaptive Remeshing Finite Element Method for Dusty Shock Flows," *International Journal of Shock Waves*, Vol. 4, No. 1, 1994, pp. 31–41.

[6] Schaaf, S. A., and Chambré, P. L., "The Flow of Rarefied Gases," *Section H of Fundamentals of Gas Dynamics*, edited by H. W. Emmons, Princeton Univ. Press, Princeton, NJ, 1958.

[7] Zarin, N. A., "Measurement of Non-Continuum and Turbulence Effects on Subsonic Sphere Drag," NASA CR-1585, June 1970.

[8] Schlichting, H., *Boundary Layer Theory*, Springer–Verlag, Berlin, 1979.

[9] Hoerner, S. F., *Fluid-Dynamic Drag*, published by Hoerner, S. F., Midland Park, NJ, 1958.

[10] Crowe, C. T., "Drag Coefficient of Particles in Rocket Nozzle," *AIAA Journal*, Vol. 5, No. 5, 1967, pp. 1021–1022. doi:10.2514/3.4119

[11] Crowe, C. T., Babcock, W. R., and Willoughby, P. G., "Drag Coefficient for Particles in Rarefied Low-Mach Number Flows," *Progress in Heat and Mass Transfer*, Vol. 6, Jan. 1972, pp. 419–431.

[12] Talbot, L., Cheng, R. K., Schefer, R. W., and Willis, D. R., "Thermophoresis of Particles in a Heated Boundary Layer," *Journal of Fluid Mechanics*, Vol. 101, No. 4, 1980, pp. 737–758. doi:10.1017/S0022112080001905

[13] Basset, A. B., "On the Motion of a Sphere in a Viscous Liquid," *Philosophical Transactions of the Royal Society of London*, Vol. 179A, No. 1888, pp. 43–63. doi:10.1098/rsta.1888.0003

[14] Epstein, P. S., "Zur Theorie des Radiometers," *Zeitschrift fuer Physik*, Vol. 54, No. 4, 1929, pp. 537–563.

[15] Phillips, W. F., "Drag on a Small Sphere Moving Through a Gas," *Physics of Fluids*, Vol. 18, No. 9, 1975, pp. 1089–1093. doi:10.1063/1.861292

[16] Millikan, R. A., "Coefficients of Slip in Gasses and the Law of Reflection of Molecules from the Surface of Solids and Liquids," *Physical Review*, Vol. 21, No. 3, 1923, pp. 217–238. doi:10.1103/PhysRev.21.217

[17] Millikan, R. A., "The Isolation of an Ion: A Precision Measurement of Its Charge and the Correction of Stokes's Law," *Physical Review*, Vol. 32, No. 4, 1911, pp. 349–397.

[18] Benson, C. M., Levin, D. A., Zhing, J., Gimelshein, S. F., and Montaser, A., "Kinetic Model for Simulation of Aerosol Droplets in High-Temperature Environments," *Journal of Thermophysics and Heat Transfer*, Vol. 18, No. 1, 2004, pp. 122–134. doi:10.2514/1.1264

[19] Stadler, J. R., and Zurick, V. J., "Theoretical Aerodynamic Characteristics of Bodies in Free-Molecule Flow Field," NACA TN 2423, July 1951, p. 12.

[20] Hersch, A. S., Friichtenicht, J. F., and Slattery, J. C., "Drag of Microscopic Spheres in Free-Molecule Flow," *Sixth International Symposium on Rarefied Gas Dynamics*, Vol. 1, Academic Press, New York, 1969, pp. 757–766.

[21] Carlson, D. J., and Hoglund, R. F., "Particle Drag and Heat Transfer in Rocket Nozzles," *AIAA Journal*, Vol. 2, No. 5, 1964, pp. 1980–1984.

[22] Henderson, C. B., "Drag Coefficients of Spheres in Continuum and Rarefied Flows," *AIAA Journal*, Vol. 14, No. 6, 1976, pp. 707–708. doi:10.2514/3.61409

[23] Hermsen, R. W., "Review of Particle Drag Models," *JANAF Performance Standardization Subcommittee 12th Meeting Minutes*, Chemical Propulsion Information Agency, Columbia, MD, 1979, p. 113.

[24] Aerosty, J., "Sphere Drag on a Low Density Flow," Univ. Of California Berkeley, Rept. HE-150-192, Jan. 1962.

[25] Bailey, A. B., and Hiatt, J., "Sphere Drag Coefficients for a Broad Range of Mach and Reynolds Numbers," *AIAA Journal*, Vol. 10, No. 11, 1972, pp. 1436–1440. doi:10.2514/3.50387

[26] Brock, J. R., "On the Theory of Thermal Forces Acting on Aerosol Particles," *Journal of Colloid Science*, Vol. 17, No. 8, 1962, pp. 768–780. doi:10.1016/0095-8522(62)90051-X

[27] Loyalka, S. K., "Thermophoretic Force on a Single Particle I. Numerical Solution of the Linearized Boltzmann Equation," *Journal of Aerosol Science*, Vol. 23, No. 3, 1992, pp. 291–300. doi:10.1016/0021-8502(92)90329-T

[28] Waldman, L., *Rarefied Gas Dynamics*, edited by L. Talbot, Academic Press, New York, 1961, p. 3232.

[29] Zheng, F., "Thermophoresis of Spherical and Non-Spherical Particles: A Review of Theories and Experiments," *Advances in Colloid and Interface Science*, Vol. 97, Nos. 1–3, 2002, pp. 255–278. doi:10.1016/S0001-8686(01)00067-7

[30] White, F. M., *Fluid Mechanics*, McGraw–Hill, New York, 1991.
[31] Van Dyke, M., *An Album of Fluid Motion*, Parabolic Press, Stanford, CA, 1982.
[32] Wegener, P. P., and Ashkenas, H., "Wind Tunnel Measurements of Sphere Drag at Supersonic Speeds and Low Reynolds Numbers," *Journal of Fluid Mechanics*, Vol. 10, No. 4, 1961, pp. 550–560. doi:10.1017/S0022112061000354
[33] Mishin, G. I., "Experimental Investigation of the Flight of a Sphere in Weakly Ionized Air," AIAA Paper 1997-2298, June 1997.
[34] Macrossan, M. N., "Scaling Parameters in Rarefied Flow and the Breakdown of the Navier-Stokes Equations," Department of Mechanical Engineering, University of Queensland, Tech. Rept. 2004/09, 2004.
[35] Sone, W., and Aoki, K., "Forces on a Spherical Particle in a Slightly Rarefied Gas," *Progress in Aeronautics and Astronautics, Rarefied Gas Dynamics*, Vol. 51, AIAA, New York, 1983, pp. 417–433.
[36] Yamamato, K., and Ishihara, Y., "Thermophoresis of a Spherical Particle in a Rarefied Gas of a Transition Regime," *The Physics of Fluids*, Vol. 31, Dec. 1988, pp. 3618–3624.
[37] Takata, S., Aoki, K. and Sone, Y., "Thermophoresis of a Sphere with a Uniform Temperature: Numerical Analysis of the Boltzmann Equation for Hard-Sphere Molecules," Vol. 159, Progress in Astronautics and Aeronautics, AIAA, Washington, D.C., 1994, pp. 626–639.
[38] Saxton, R. L., and Ranz, W. E., "Thermal force on an aerosol particle in a temperature gradient," *Journal of Applied Physics*, Vol. 23, Aug. 1952, pp. 917–923. doi:10.1063/1.1702330
[39] Schmitt, K. H.,"Untersuchungen an Schwebstoffteilchen im Temperaturfeld," *Zeitschrift fuer Naturforschung*, Vol. 14a, 1959, pp. 870–881.
[40] Schadt, C. F., and Cadle, R. D., "Thermal Forces on Aerosol Particles," *Journal of Physical Chemistry*, Vol. 65, No. 10, 1961, pp. 1689–1694. doi:10.1021/j100827a006
[41] Jacobson, S., and Brock, J. R., "The Thermal Force on Spherical Sodium Chloride Aerosols," *Journal of Colloid Science*, Vol. 20, No. 6, 1965, pp. 544–554. doi:10.1016/0095-8522(65)90034-6
[42] Li, W., and Davis, E. J., "Measurement of the Thermophoretic Force by Electrodynamic Levitation: Microspheres in Air," *Journal of Aerosol Science*, Vol. 26, No. 7, 1995, pp. 1063–1083. doi:10.1016/0021-8502(95)00047-G

R. Rangel
Associate Editor